

Continuous-time scheduling of a hydrothermal system with integration of offshore wind power

Mari Lund Øvstebø^{*†}, Christian Øyn Naversen^{*}, Arild Helseth[‡] and Hossein Farahmand^{*}

^{*}Department of Electric Power Engineering, NTNU – Trondheim, Norway

[‡]Department of Energy Systems, SINTEF Energy Research – Trondheim, Norway

[†]Corresponding author: mariovs@stud.ntnu.no

Abstract—In this work, a continuous-time unit commitment formulation of a hydrothermal system with integration of offshore wind power is used to model the North European system operation. The cost of covering the structural imbalances in the system is quantified by a cost comparison to an analogous discrete-time model. If the discrete-time unit commitment is implemented for real-time operation, 55 MWh (0.22%) load shedding should be introduced since the demand in periods with high net-load ramping cannot be met. The simulation results demonstrate that the proposed framework reduces system balancing cost and the events of ramping scarcity in the real-time balancing.

Index Terms—Continuous-time optimization, Hydrothermal scheduling, Offshore wind power, Unit commitment

I. INTRODUCTION

A significant amount of offshore wind power is expected to be integrated into the European power system in the coming years [1]. The variable nature of wind power generation challenges the security of the power system as the flexibility of conventional generators are pushed to their limits. Cascaded hydropower is an existing flexible energy storage technology which can provide energy and flexibility on a system scale, and the Nordic countries have considerable amounts of hydropower installed in their current power systems. Several high voltage direct current (HVDC) cables between Norway and continental Europe (Netherlands and Denmark) have been constructed in recent years, and new interconnectors to Germany and Great Britain are under construction. The increased transmission capacity makes it possible to use Norwegian hydropower resources to help balance the wind power in the North European power system. Hydrothermal coordination in the presence of uncertain wind power generation has been studied in the literature, which includes both models with long time horizons [2]–[5] and short-term studies [6].

The discrete structure of the European day-ahead electricity markets cannot prevent the occurrence of a mismatch between the market cleared volumes and the actual production and consumption. These structural imbalances must be balanced in real-time by activating procured reserve capacity. As wind power can vary quickly and unpredictably within the span of a few minutes, the structural imbalances and need for balancing can be worsened by a high wind power penetration. Continuous-time optimization is a way of formulating the standard unit commitment and economic dispatch problems

with continuously varying time-dependent variables and input data, originally formulated for a purely thermal system in [7]. The continuous-time framework has since been extended to incorporate energy storage technology in [8], and multi-stage stochastic unit commitment and reserve scheduling models are developed in [9] and [10]. In previous work, we have derived the formulation of the cascaded hydropower constraints in the continuous-time framework [11]. This paper extends the model presented in [11] to include wind power generation. The main contributions of the paper are:

- Quantifying the cost of structural imbalances in a test system resembling the Northern European power system by comparing the costs obtained by a continuous-time unit commitment model and an analogous discrete-time model.
- Identifying specific periods where the discrete-time model overestimates the flexibility of the system. This is done by simulating operation with a continuous-time model, setting the binary commitment decisions equal to the discrete-time solution.

Section II defines the continuous-time model in detail, while the case study and results are presented in Section III. A concluding summary is found in Section IV.

II. MODEL

The mathematical formulation of the continuous-time model is based on [11]. In this paper, the model is extended to include offshore wind power, hence constraints for wind power production and wind curtailment are added to the model.

A. Continuous-time optimization framework

The continuous-time optimizations framework directly models sub-hourly variations by representing all time-varying data and variables as polynomials of time, which allows ramping and other inter-temporal constraints to be enforced continuously. Several spline models can be used to approximate the continuous-time trajectory curve of a data set, where the accuracy of the spline model is dependent on the order of the basis. A convenient spline model is the Bernstein polynomials, where the time dependent decision variables will be defined by using the Bernstein polynomials of degree n , which form a basis for any polynomials of degree equal or less than n on the interval $t \in [0, 1]$. For a given time interval $h \in \mathcal{T}$

with length δ_h , a time-varying decision variable $x(t)$ can be expressed as:

$$x(t) = \mathbf{x}_h^T \cdot \mathbf{B}_n \left(\frac{t - T_h}{\delta_h} \right), \quad T_h \leq t \leq T_{h+1}, \quad (1)$$

where $T_h = \sum_{i < h} \delta_i$ is the start time of interval h , \mathbf{x}_h is a vector of $n + 1$ Bernstein polynomial coefficients and $\mathbf{B}_n(t)$ is the vector of Bernstein polynomials of degree n . This definition gives a piece-wise polynomial description of time-dependent variables where the polynomial coefficients \mathbf{x}_h become the decision variables in the optimization problem. Choosing Bernstein polynomials of degree zero recovers the usual discrete-time formulation of piece-wise constant variables.

In this paper, the Bernstein polynomials of degree three will be used as a basis for each time interval h :

$$\mathbf{B}_3(t) = [(1-t)^3, 3t(1-t)^2, 3t^2(1-t), t^3]. \quad (2)$$

This degree of freedom allows the application of C^1 continuity constraints between time intervals without drastically increasing the number of decision variables in the model. The C^1 continuity constraints can be expressed with the use of the Bernstein coefficients of the decision vector \mathbf{x} , where the coefficients can be labeled as \mathbf{x}^i for $i \in \{0, 1, 2, 3\}$. With this in mind, the continuity constraints can be expressed as:

$$\mathbf{x}_h^3 = \mathbf{x}_{h+1}^0 \quad \forall h \in \mathcal{T} \setminus \{N\} \quad (3)$$

$$\mathbf{x}_h^3 - \mathbf{x}_h^2 = \mathbf{x}_{h+1}^1 - \mathbf{x}_{h+1}^0 \quad \forall h \in \mathcal{T} \setminus \{N\}. \quad (4)$$

The result of integrating and differentiating $\mathbf{B}_n(t)$ can be represented by Bernstein polynomials of degree $\mathbf{B}_{n+1}(t)$ and $\mathbf{B}_{n-1}(t)$, respectively. These relationships are described by the linear matrices \mathbf{K} and \mathbf{N} for $\mathbf{B}_3(t)$ in eqs. (5) and (6). Another useful relation is the definite integral of the polynomials over the whole interval, shown in eq. (7).

$$\dot{\mathbf{B}}_3(t) = \mathbf{K} \cdot \mathbf{B}_2(t) \quad (5)$$

$$\int \mathbf{B}_3(t) dt = \mathbf{N} \cdot \mathbf{B}_4(t) \quad (6)$$

$$\int_0^1 \mathbf{B}_3(t) dt = \frac{1}{4} \cdot \mathbf{1} \quad (7)$$

These properties, together with the convex hull property, are some of the main reasons for using Bernstein polynomials in the continuous-time optimization framework. The convex hull property makes it possible to impose inequality constraints on the decision variable $x(t)$ by directly bounding the coefficient \mathbf{x}_h . For a more detailed introduction to continuous-time optimization in power systems, the reader is referred to for instance [7].

B. Mathematical formulation of continuous-time UC

1) *Thermal constraints:* The following constraints are defined for all thermal units $i \in \mathcal{I}$ over time intervals $h \in \mathcal{T}$. $u_i(t)$, $SU_i(t)$ and $SD_i(t)$ are binary variables describing the

commitment status, startup and shutdown of thermal generator i , respectively. Constraints (8) and (9) ensure that the thermal generator can ramp up the production, $g_i(t)$, from zero to above G_i^{min} , or ramp down production to zero, during time interval h . This smooth ramping of the production is necessary when the continuity constraints for the thermal production variable will be applied in II-B4. Limitations on the derivative $\dot{g}_i(t)$ are imposed in (10) and (11) such that the ramping of the thermal production stays within specified limits R_i^u and R_i^d by utilizing property (5). When there is a startup or a shutdown, the ramping limit is increased to G_i^{max} . Constraints (12) and (13) counts the number of startup and shutdown events.

$$G_i^{min} \mathbf{u}_{i,h} \leq \mathbf{g}_{i,h} \leq G_i^{max} \mathbf{u}_{i,h} \quad (8)$$

$$\mathbf{u}_{i,h} = [u_{i,h}, u_{i,h}, u_{i,h+1}, u_{i,h+1}]^T \quad (9)$$

$$\frac{1}{\delta_h} \mathbf{g}_{i,h}^T \cdot \mathbf{K} \leq (R_i^u + (G_i^{max} - R_i^u) SU_{i,h}) \mathbf{1}^T \quad (10)$$

$$\frac{1}{\delta_h} \mathbf{g}_{i,h}^T \cdot \mathbf{K} \geq -(R_i^d + (G_i^{max} - R_i^d) SD_{i,h}) \mathbf{1}^T \quad (11)$$

$$SU_{i,h} - SD_{i,h} = u_{i,h+1} - u_{i,h} \quad (12)$$

$$SU_{i,h} + SD_{i,h} \leq 1 \quad (13)$$

$$u_{i,h}, SU_{i,h}, SD_{i,h} \in \{0, 1\} \quad (14)$$

2) *Hydropower constraints:* The constraints from (15) to (30) are added to the optimization problem for the hydro area and are defined for all hydropower plants $m \in \mathcal{M}$ over time intervals $h \in \mathcal{T}$.

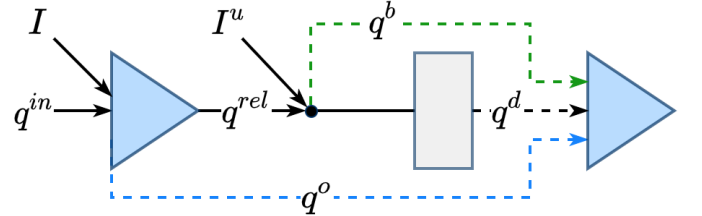


Fig. 1. A rotated illustration of the waterways between reservoirs together with regulated and unregulated natural inflow.

$$v_{m0} = V_m^0 \quad (15)$$

$$v_{m,h+1} - v_{m,h} = \frac{1}{4} \delta_h \mathbf{1}^T \cdot \mathbf{q}_{m,h}^{net} \quad (16)$$

$$\mathbf{0} \leq v_{m,h} \mathbf{1} + \delta_h \mathbf{N}^T \cdot \mathbf{q}_{m,h}^{net} \leq V_m \mathbf{1} \quad (17)$$

$$\mathbf{q}_{m,h}^{in} = \sum_{j \in \mathcal{J}_m^d} \sum_{n \in \mathcal{N}_j} \mathbf{q}_{j,n,h}^d + \sum_{j \in \mathcal{J}_m^b} \mathbf{q}_{j,h}^b + \sum_{j \in \mathcal{J}_m^o} \mathbf{q}_{j,h}^o \quad (18)$$

$$\mathbf{q}_{m,h}^{net} = \mathbf{I}_{m,h} + \mathbf{q}_{m,h}^{in} - \mathbf{q}_{m,h}^{rel} - \mathbf{q}_{m,h}^o \quad (19)$$

$$\mathbf{q}_{m,h}^{rel} = \sum_{n \in \mathcal{N}_m} \mathbf{q}_{m,n,h}^d + \mathbf{q}_{m,h}^b - \mathbf{I}_{m,h}^u \quad (20)$$

$$\mathbf{0} \leq \mathbf{q}_{m,h}^b \leq Q_m^b \cdot \mathbf{1} \quad (21)$$

$$\mathbf{0} \leq \mathbf{q}_{m,h}^o \quad (22)$$

$$\mathbf{0} \leq \mathbf{q}_{m,h}^{rel} \quad (23)$$

$$\mathbf{p}_{m,h} = \sum_{n \in \mathcal{N}_m} \eta_{m,n} \mathbf{q}_{m,n,h}^d \quad (24)$$

$$Q_{m,n}^d w_{m,n,h} \mathbf{1} \leq \mathbf{q}_{m,n,h}^d \leq Q_{m,n}^d \mathbf{1} \quad (25)$$

$$\mathbf{q}_{m,n,h}^d \leq Q_{m,n}^d w_{m,n-1,h} \mathbf{1} \quad (26)$$

$$P_m^{\min} z_{m,h} \mathbf{1} \leq \mathbf{p}_{m,h} \leq P_m^{\max} z_{m,h} \mathbf{1} \quad (27)$$

$$SU_{m,h} - SD_{m,h} = z_{m,h+1} - z_{m,h} \quad (28)$$

$$SU_{m,h} - SD_{m,h} \leq 1 \quad (29)$$

$$z_{m,h}, SU_{m,h}, SD_{m,h} \in \{0, 1\}. \quad (30)$$

v_{mh} is the instantaneous volume at the beginning of interval h for reservoir m , and constraint (15) sets the initial volume for each reservoir. Constraint (16) calculates the change in volume between two time intervals by integrating the net inflow, $q_m^{\text{net}}(t)$, over the entire time interval by the use of (7). Constraint (17) bounds the reservoir volume within the time interval, found by using property (6), between zero and the maximal reservoir volume V_m . Figure 1 shows that the waterways of the cascaded system is modelled by three separate routes: the spill gate, $q_m^o(t)$, the bypass gate, $q_m^b(t)$, and the discharge through each turbine segment $n \in \mathcal{N}_m$, $q_{m,n}^d(t)$. The hydropower topology constraints, expressed in (18) to (23), implement this system description. $I_m(t)$, $I_m^u(t)$ and $q_m^{\text{net}}(t)$ represents regulated and unregulated natural inflow, and net flow into the reservoir, respectively. $q_m^{\text{in}}(t)$ is the sum of the controlled flow into the reservoir from the upstream system, while $q_m^{\text{rel}}(t)$ is the total released flow out of the reservoir. Q_m^b denotes the maximal bypass flow. The constraints for hydropower production and commitment is expressed in (24) to (30), where $p_m(t)$ is the generated hydropower. The conversion from discharge through the turbine to generated power is a non-linear function depending on the plant head and the efficiency curves of the generator and the turbine. In (24), this non-linear function is approximated as a piece-wise linear curve, where each segment of the discharge variable has a constant efficiency η_n . As discussed in [11], binary variables $w_{m,n}(t)$ are necessary in the continuous-time formulation to ensure that the discharge segments are uploaded in physically correct order. Constraint (25) and (26) bound the flow through each discharge segment within an upper and lower limit with the use of the binary variable, and these two constraints are defined for all discharge segments $n \in \mathcal{N}_m$.

Constraint (27) to (30) expresses the hydropower unit commitment constraints, where $z_m(t)$, $SU_m(t)$ and $SD_m(t)$ are binary variables describing the commitment status, startup and shutdown of a hydropower unit m , respectively. From constraint (27), it can be seen that all the Bernstein coefficients in the decision variable $p_m(t)$ for a given hour are related to the commitment of the generator in that given hour. This forces the hydropower unit commitment decision to be constant during a time interval h , and will ensure that the production never is between zero and P_m^{\min} . Unlike the smooth operation enforced on the thermal generators, discontinuous jumps in the hydropower production curve when there are startups and shutdowns are therefore permitted.

3) *Wind Power and System constraints:* Area and system wide constraints in the model are the following:

$$\mathbf{0} \leq \mathbf{s}_{a,h} \leq \mathbf{W}_{a,h} \quad (31)$$

$$\rho_{a,h}^c = \mathbf{W}_{a,h} - \mathbf{s}_{a,h} \quad (32)$$

$$\alpha \geq \sum_{m \in \mathcal{M}} WV_{m,k} v_{m,N+1} + D_k \quad (33)$$

$$-F_l^{\max} \mathbf{1} \leq \mathbf{f}_{l,h} \leq F_l^{\max} \mathbf{1} \quad (34)$$

$$\sum_{m \in \mathcal{M}_a} \mathbf{p}_{m,h} + \sum_{i \in \mathcal{I}_a} \mathbf{g}_{i,h} + \mathbf{s}_{a,h} - \sum_{l \in \mathcal{L}} G_{l,a} \mathbf{f}_{l,h} = \mathbf{L}_{a,h} - \rho_{a,h}^s. \quad (35)$$

Constraint (31) and (32) expresses the wind power generation $s_a(t)$ and the wind curtailment $\rho_a^c(t)$, respectively, where both constraints are defined over time intervals $h \in \mathcal{T}$ and areas $a \in \mathcal{A}$. Generated wind power is bound within zero and the maximal available wind power curve $W(t)$. The future expected operating cost for the system, α , which is directly added to the objective function in (37), is bounded by constraint (33), which are a set of linear Benders cuts $k \in \mathcal{K}$. The cut coefficients $WV_{m,k}$ and the cut constants D_k can be calculated by long-term hydrothermal models such as the one in [12], and the future expected system cost ultimately depends on the end volume of water in each reservoir. The power flow on the HVDC cables, $f_l(t)$, is bound by a maximal flow limit F_l^{\max} in (34), defined for all lines $l \in \mathcal{L}$ over time intervals $h \in \mathcal{T}$. Constraint (35) shows the power balance, which needs to be satisfied for each area $a \in \mathcal{A}$ over time intervals $h \in \mathcal{T}$. \mathcal{M}_a and \mathcal{I}_a are the sets of hydropower and thermal units located in area a , and $G_{l,a}$ is the adjacency matrix of the HVDC grid. $L_a(t)$ is the area load and $\rho_a^s(t)$ is the amount of load shedding within each area.

4) *Continuity constraints:* One important aspect of the continuous-time optimization framework is that the value of the decision variable and its derivative can be continuous over time interval shifts. The continuity constraints in (3) and (4) are added to the optimization problem for the thermal production decision variable $\mathbf{g}_{i,h}$, the offshore wind production decision variable $\mathbf{s}_{a,h}$ and for the power flow decision variable $\mathbf{f}_{l,h}$ for all times $h \in \mathcal{T}$. This enforces C^1 continuity, meaning that the curves have continuous values and derivatives for all points in time. Less strict continuity constraints are added for the variables connected to the hydropower units $m \in \mathcal{M}$ over time intervals $h \in \mathcal{T}$, which is discussed in more detail in [11]. The C^0 continuity constraint in (3) is applied to the flow through the bypass gate and spill gate, $\mathbf{q}_{m,h}^b$ and $\mathbf{q}_{m,h}^o$. As there is need for discontinuous jumps in the hydropower production during startups and shutdowns, enforcing C^0 continuity on $\mathbf{p}_{m,h}$ will not be possible. Instead, constraint (3) is replaced with the inequality constraints in (36), which makes the hydropower production C^0 continuous over time interval changes except if a startup or shutdown occurs:

$$-P_m^{\max} SU_{m,h} \leq \mathbf{p}_{m,h}^3 - \mathbf{p}_{m,h+1}^0 \leq P_m^{\max} SD_{m,h}. \quad (36)$$

5) *Objective function*: The objective function for the proposed model, presented in (37), is to minimize the total cost of the system. The total cost includes the future expected cost of the hydro system, α , the cost of spilling and bypassing water, and the operational, startup and shutdown costs for the thermal generators. In addition, a negligible penalty for curtailment of wind power and a high penalty for load shedding are included in the last line. Both startup and shutdown costs for the hydropower plants and the wind farms are assumed to be negligible in this model.

$$\begin{aligned}
Z = & \alpha + \frac{1}{4} \sum_{m \in \mathcal{M}} \sum_{h \in \mathcal{T}} \delta_h \mathbf{1}^T \cdot (C^b \mathbf{q}_{m,h}^b + C^o \mathbf{q}_{m,h}^o) \\
& + \sum_{i \in \mathcal{I}} \sum_{h \in \mathcal{T}} \left(\frac{1}{4} \delta_h C_i \mathbf{1}^T \cdot \mathbf{g}_{i,h} + C_i^{start} SU_{i,h} + C_i^{stop} SD_{i,h} \right) \\
& + \frac{1}{4} \sum_{h \in \mathcal{T}} \delta_h \mathbf{1}^T \cdot (C^c \boldsymbol{\rho}_h^c + C^s \boldsymbol{\rho}_h^s) \quad (37)
\end{aligned}$$

III. CASE STUDY

A case study of a stylized three-area system resembling Northern Europe is presented in this section. The continuous-time model presented in Section II and an analogous discrete-time model are both solved to compare how the different components in the system reacts when variable offshore wind power is integrated into the power system. Both models have been implemented in Pyomo and solved with CPLEX 12.10.

A. System topology and input data

The stylized three-area system contains a hydro dominated Norwegian area, a thermal dominated Central European area and an offshore wind area in the North Sea, connected through HVDC cables. The hydropower area is based on a real Norwegian cascaded system containing 12 reservoirs and plants with a total hydropower production capacity of 535 MW. A detailed description of the hydropower topology can be found in [13]. The ratio between the capacity of the cascaded system and the total installed capacity in Norway (32 257 MW at the beginning of 2019 [14]), here referred to as the system scaling rate, is used to scale the capacities for the rest of the generation units and cables in the three-area system. The installed capacity of the offshore wind area and the wind series used in the case study is based on wind data from Denmark, found in [15], and scaled to match the total offshore wind capacity provided by Denmark, Germany and the Netherlands in the North Sea. The wind farms in the offshore wind area are clustered together as one big wind farm, with a total installed capacity of 172 MW after it is scaled down with the system scaling rate. The thermal area contains 104 thermal generators, divided into five groups after the primary-fuel; fossil gas, fossil hard coal, lignite, nuclear and fossil oil generators. The ramping capabilities, installed capacity and marginal, startup, and shutdown costs are based on operating thermal generators in Germany and the Netherlands [16], [17]. The total capacity of the thermal area is 921 MW after scaling. The three-area system is connected through two HVDC cables, where the

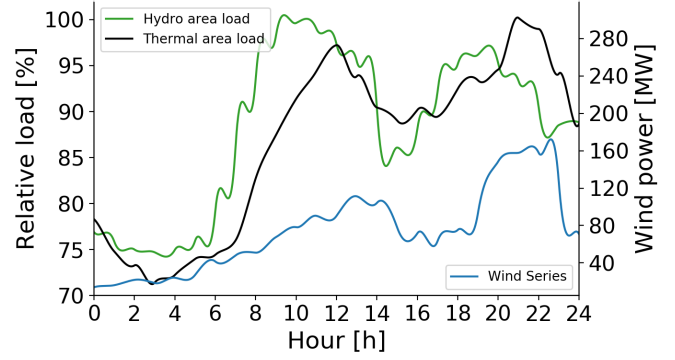


Fig. 2. The continuous-time load profiles of thermal and hydro areas scaled by the value of the peak load (left axis) together with the continuous-time wind power series for the offshore wind area (right axis).

hydro and the thermal area are connected by a 63 MW cable and the offshore wind area and the thermal area are connected by a 172 MW cable. The capacity of the cable connecting the thermal and the hydro area is based on the total installed capacity of the interconnectors between Norway and mainland Europe today [18], [19], including the 1400 MW Nordlink cable, which will be installed during 2020 [20]. This results in 63 MW of transmission capacity after it is scaled down with the system scaling rate. The interconnector capacity between the thermal area and the offshore wind area is assumed to be equal to the installed capacity of the offshore wind area, to ensure no limitations on the utilization of the possible offshore wind power production. The time horizon is set to 24 hours, with hourly time intervals in the continuous-time model. The discrete-time model has quarterly time intervals but hourly commitment decisions. The case study is based on data from 22/4-2019 where the reservoir volume in Norway was at 31.6%, its lowest during 2019 [21]. Fig. 2 shows the wind series for the offshore wind area and the load profiles for the demand in the other areas. For the thermal area, it is assumed that the peak load is 85% of the installed capacity, which implies a peak load of 783 MW. The hydro area has a peak load of 400 MW which is 75% of the installed capacity. The load profiles are based on data from Nord Pool [22] and ENTSO-E [23]. The offshore wind area has a peak wind production of 163.54 MW, where the wind series is based on data from [15]. The continuous time load and wind series are calculated from the data by a least-squares error fit to the Bernstein polynomials. For the piece-wise constant load and wind series, the average quarterly values are used.

B. Continuous-time and discrete-time model comparison

Both the discrete-time model and the continuous-time model are solved to optimality, meaning an absolute mip-gap of 0% was reached. The discrete-time model was solved within 80 sec., while the continuous-time model used 2 378 sec. to reach optimality on a single core 2.4 GHz machine. A breakdown of the objective function costs is listed in Table I.

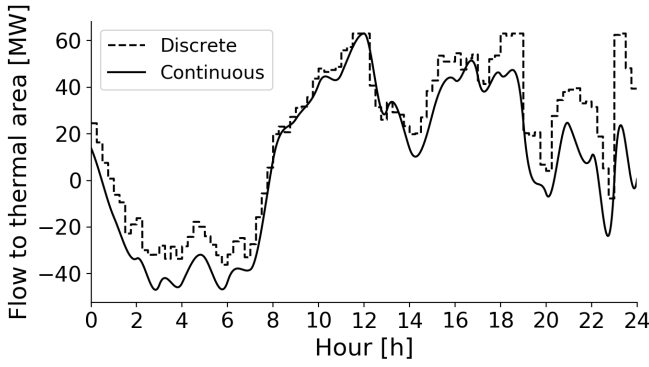


Fig. 3. Power flow on the HVDC cable from the hydro area to the thermal area.

For the thermal area, the discrete-time model schedules 51 generators to be committed during the whole optimization horizon. All fossil hard coal, lignite and nuclear generators are operating to cover the base load, while three fossil gas generators and zero oil-fired generators are committed. Six additional gas-fired generators are committed to meet the net-load variations in the continuous-time model. This result highlights that the continuous-time model sees the need to commit extra flexible units to cover sub-hourly net-load variations and peaks. This results in a 3.68% higher thermal cost and a 2.12% higher scheduled thermal production than in the discrete-time model. From Fig. 3 it can be seen that the power flow from the hydro area to the thermal area is higher for the discrete-time model during periods when the total load of the system is high, especially at the end of the scheduling period. This results in a 3.15% higher scheduled hydropower production and 2.15% higher hydropower related costs in the discrete-time model. Also note the rapid flow change in hour 23 in the discrete-time model caused by the drop in wind power production, which is not seen in the continuous-time solution. It is clear that such an abrupt change in flow is either infeasible or very costly when thermal generation and line flow continuity is enforced. The offshore wind power utilization is high entire scheduling period for both models, though a small amount of wind power is curtailed in the continuous-time model. Overall, the total cost of the system will be higher for the continuous-time model, with a 3 774.6 € /day (0.53%) increase compared to the discrete-time model.

TABLE I
COMPARISON OF THE TOTAL SYSTEM COSTS. ROW 3-5 REPRESENTS THE COST OF LINE 1-3 IN (37), RESPECTIVELY.

Cost	Discrete-time	Continuous-time
Objective value [€]	713 092.4	716 867.1
Hydro related costs [€]	388 795.7	380 623.0
Thermal related costs [€]	324 296.7	336 241.8
Curtailement and shedding costs [€]	0.0	2.3

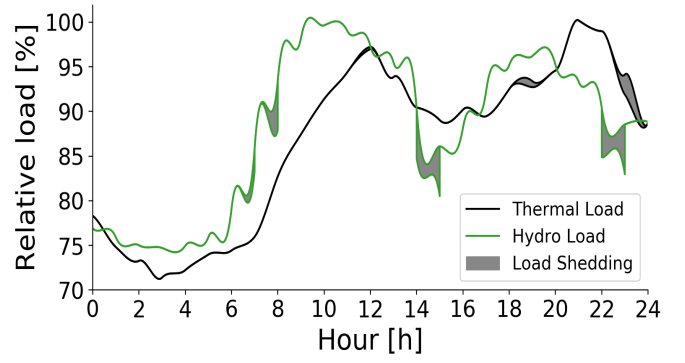


Fig. 4. Load shedding when the continuous-time model is solved with the fixed commitment solution from the discrete-time model.

C. Continuous-time simulator for real-time operation

To investigate where the discrete-time model overestimates the flexibility of the system, the continuous-time model is used as a simulator for real-time operation. The unit commitment decisions from the discrete-time model is used as input to the continuous-time model to identify in which periods the discrete-time model overestimates the system flexibility. From Fig. 4, it can be seen that the discrete-time model fails to commit enough units in periods when there are rapid changes in load and wind power. In these periods, an imbalance between the generated power and the actual load will occur, which will manifest as load shedding in the presented model. In total, 55 MWh load shedding will take place during the entire scheduling period, where the largest amount occurs in the hydropower area. This means that 0.22% of the total load will not be covered by the committed generators. In real system operations, the system operators need to activate reserves in these periods to balance the power system.

IV. CONCLUSION

We assess the structural imbalances in the interconnected North European power system by solving a continuous-time hydrothermal model with offshore wind power, and compare the results to an analogous discrete-time model. The increased cost of balancing the sub-hourly variations in the net-load was found to be 0.53% of the discrete-time model system costs per day. This cost increase is due to the overestimation of the system flexibility in the discrete-time model. The specific periods where the discrete-time model formulation overestimates the system flexibility were pinpointed by fixing the binary unit commitment decisions of the continuous-time model to be equal to the optimal discrete-time commitment solution. This resulted in a total of 55 MWh of load which could not be covered by the committed units and represents an additional requirement for fast system reserves that are not needed in the continuous-time solution.

V. ACKNOWLEDGMENTS

This work was funded by the Research Council of Norway, Project No. 268014/E20.

REFERENCES

- [1] “Offshore Wind Outlook 2019 – Analysis - IEA.” [Online]. Available: <https://www.iea.org/reports/offshore-wind-outlook-2019>
- [2] T. Aigner, S. Jaehnert, G. L. Doorman, and T. Gjengedal, “The effect of large-scale wind power on system balancing in Northern Europe,” *IEEE Trans. Sustain. Energy*, vol. 3, no. 4, pp. 751–759, 2012.
- [3] A. Helseth, A. Gjelsvik, B. Mo, and U. Linnet, “A model for optimal scheduling of hydro thermal systems including pumped-storage and wind power,” *IET Gener. Transm. Distrib.*, vol. 7, no. 12, pp. 1426–1434, 2013.
- [4] H. Farahmand, S. Jaehnert, T. Aigner, and D. Huertas-Hernando, “Nordic hydropower flexibility and transmission expansion to support integration of North European wind power,” *Wind Energy*, vol. 18, no. 6, pp. 1075–1103, jun 2015.
- [5] M. N. Hjelmeland, C. T. Larsen, M. Korpås, and A. Helseth, “Provision of rotating reserves from wind power in a hydro-dominated power system,” in *2016 Int. Conf. Probabilistic Methods Appl. to Power Syst.* IEEE, oct 2016, pp. 1–7.
- [6] B. P. Cotia, C. L. Borges, and A. L. Diniz, “Optimization of wind power generation to minimize operation costs in the daily scheduling of hydrothermal systems,” *Int. J. Electr. Power Energy Syst.*, vol. 113, pp. 539–548, dec 2019.
- [7] M. Parvania and A. Scaglione, “Unit Commitment With Continuous-Time Generation and Ramping Trajectory Models,” *IEEE Trans. Power Syst.*, vol. 31, no. 4, pp. 3169–3178, jul 2016.
- [8] R. Khatami, M. Parvania, and P. P. Khargonekar, “Scheduling and Pricing of Energy Generation and Storage in Power Systems,” *IEEE Trans. Power Syst.*, vol. 33, no. 4, pp. 4308–4322, jul 2018.
- [9] K. Hreinsson, B. Analui, and A. Scaglione, “Continuous Time Multi-Stage Stochastic Reserve and Unit Commitment,” in *2018 Power Syst. Comput. Conf.* IEEE, jun 2018, pp. 1–7.
- [10] R. Khatami, M. Parvania, and A. Narayan, “Flexibility Reserve in Power Systems: Definition and Stochastic Multi-Fidelity Optimization,” *IEEE Trans. Smart Grid*, vol. 11, no. 1, pp. 644–654, jan 2020.
- [11] C. Ø. Naversen, A. Helseth, B. Li, M. Parvania, H. Farahmand, and J. P. S. Catalão, “Hydrothermal Scheduling in the Continuous-Time Framework,” dec 2019, accepted for publication in The Power Systems Computation Conference (PSCC) 2020. [Online]. Available: <http://arxiv.org/abs/1912.06877>
- [12] A. Helseth, B. Mo, A. L. Henden, and G. Warland, “Detailed long-term hydro-thermal scheduling for expansion planning in the Nordic power system,” *IET Gener. Transm. Distrib.*, vol. 12, no. 2, pp. 441–447, jan 2018.
- [13] C. Ø. Naversen, H. Farahmand, and A. Helseth, “Accounting for reserve capacity activation when scheduling a hydropower dominated system,” *Int. J. Electr. Power Energy Syst.*, vol. 119, p. 105864, jul 2020.
- [14] Accessed 10/1-2019. [Online]. Available: <https://www.nve.no/energiforsyning/kraftproduksjon/vannkraft/?ref=mainmenu>
- [15] Accessed 2/6-2019. [Online]. Available: https://www.energidataservice.dk/en/dataset/electricityprodex5minrealtime/resource_extract/06380963-b7c6-46b7-aec5-173d15e4648b
- [16] Accessed 2/6-2019. [Online]. Available: <https://www.eex-transparency.com/power/de/production/capacity/>
- [17] Accessed 2/6-2019. [Online]. Available: <https://www.energy-charts.de/osm.htm>
- [18] Accessed 2/6-2019. [Online]. Available: https://www.nexans.no/eservice/Norway-en/navigatepub_142640_-34274/Royal_opening_of_Skagerrak_4.html
- [19] J. Skog, K. Koreman, B. Pääjärvi, and T. Andersröd, “The NORNED HVDC cable link—a power transmission highway between norway and the netherlands,” *ENERGEX 2006, Stavanger, Norway*, 01 2006.
- [20] Accessed 2/6-2019. [Online]. Available: <https://www.statnett.no/en/about-statnett/news-and-press-releases/News-archive-2018/norwegian-german-power-cable-being-installed/>
- [21] Accessed 3/3-2019. [Online]. Available: <https://www.statnett.no/en/for-stakeholders-in-the-power-industry/data-from-the-power-system/#hydrological-data>
- [22] Accessed 2/6-2019. [Online]. Available: <https://www.nordpoolgroup.com/Market-data1/Power-system-data/Consumption1/Consumption/NO/Hourly1/?view=table>
- [23] Accessed 2/6-2019. [Online]. Available: <https://transparency.entsoe.eu/load-domain/r2/totalLoadR2/show>